

Nematicity, magnetism and superconductivity in FeSe under pressure: Unified explanation based on the self-consistent vertex correction theory

Youichi Yamakawa, and Hiroshi Kontani

Department of Physics, Nagoya University, Furo-cho, Nagoya 464-8602, Japan.

(Dated: April 20, 2022)

To understand the rich electronic phase diagram in FeSe under pressure that vividly demonstrates the strong interplay between the nematicity, magnetism and superconductivity, we analyze the electronic states by including the higher-order many-body effects called the vertex correction (VC). We predict the pressure-induced emergence of xy -orbital hole-pocket based on the first-principles analysis. Due to this pressure-induced Lifshitz transition, the spin fluctuations on the xy orbital are enhanced, whereas those on xz, yz orbitals are gradually reduced. For this reason, nonmagnetic orbital order $O = n_{xz} - n_{yz}$, which is driven by the spin fluctuations on xz, yz orbitals through the intra-orbital VCs, is suppressed, and it is replaced with the magnetism of xy -orbital d -electrons. The nodal s -wave state at ambient pressure ($O \neq 0$) and the enhancement of T_c under pressure are driven by the cooperation between the spin and orbital fluctuations.

PACS numbers: 74.70.Xa, 75.25.Dk, 74.20.Pq

INTRODUCTION

Close relationship between the nematicity, magnetism, and high- T_c superconductivity is an essential electronic properties in Fe-based superconductors. The nematic transition is the rotational symmetry breaking in the electronic states at T_{str} , and the strong nematic fluctuations are observed above T_{str} [1–3]. Inside the nematic phase below T_{str} , large orbital polarization ($E_{yz} - E_{xz} \sim 60\text{meV}$) is observed by ARPES studies [4]. As the nematic order parameter, the spin-nematic order [5, 6] and orbital/charge order [8–10] have been discussed actively. In both scenarios [5, 6, 10], the nematicity and magnetism are closely related, so the magnetic transition slightly below T_{str} observed in many Fe-based superconductors is naturally explained.

To uncover the origin of the nematicity in Fe-based superconductors, very rich phase diagram of FeSe attracts increasing attention. Above $T_{\text{str}} = 90\text{K}$ in FeSe at ambient pressure, strong nematic fluctuations emerges whereas low-energy spin fluctuations are weak [11–14]. In the nematic state below T_{str} , large orbital polarization emerges [15–20], whereas no magnetism appears down to the superconducting temperature $T_c = 9\text{K}$. Both the spin nematic [21–24] and the orbital order [25–29] scenarios have been applied for FeSe so far. In the latter scenario, the orbital nematicity is unable to be explained unless the higher-order electronic correlations beyond the mean-field, called the vertex corrections (VCs), is taken into consideration. Recently, it was revealed that the Aslamazov-Larkin (AL) type VC, which expresses the strong interference between the orbital and spin fluctuations, gives rise to the nematicity due to the orbital order $O = n_{xz} - n_{yz}$. The nontrivial “sign-reversal orbital polarization” observed by ARPES studies below T_{str} [20] is reproduced by taking both the AL-VC and the Maki-Thompson VC [26].

The pressure-induced change in the electronic states in FeSe is an important open problem [30–37]. Under pressure, T_{str} decreases whereas T_c increases, and the nematic phase is replaced with the magnetic order ($T_m \sim 30\text{K}$) at $P = 2\text{GPa}$. This pressure-induced magnetism in FeSe may remind us of the second magnetic phase in heavy H-doped region in LaFeAsO [38]. Around 4GPa , T_m reaches its maximum (45K), and T_c in the magnetic phase exceeds 20K . It is a significant challenge for theorists to explain such rich pressure-induced electronic states based on the realistic Hubbard model for FeSe.

In this paper, we predict the pressure-induced emergence of xy -orbital hole-pocket based on the first-principles analysis. Due to this pressure-induced Lifshitz transition, the spin fluctuations on the xy orbital increase, whereas those on the xz, yz orbitals gently decrease. [10]. For this reason, nematic orbital order $n_{xz} \neq n_{yz}$, which is driven by the spin fluctuations on xz, yz orbitals through the intra-orbital VCs, is suppressed and replaced with the magnetism on the xy orbital. The nodal s -wave state at 0GPa below T_{str} [39–41] and the enhancement of T_c under high pressures are given by the orbital+spin fluctuations. The close interplay between the nematicity, magnetism, and superconductivity due to the VC in FeSe would be the universal feature of Fe-based superconductors.

In FeSe at ambient pressure, weak spin fluctuations are enough for realizing the orbital order due to the AL-VC, because of the smallness of the ratio J/U and the “absence of the xy -orbital hole-pocket” as discussed in Ref. [25]. Since the Fermi energy of each pocket is very small in FeSe, the nature of spin fluctuations is sensitively modified by the pressure-induced parameter change. Then, spin-fluctuation-driven orbital order is also sensitively modified. Therefore, rich T - P phase diagram in FeSe is naturally explained.

We study the following two-dimensional eight-orbital

Hubbard model:

$$H = H_0 + H_P + rH_U, \quad (1)$$

where H_0 is the kinetic term for FeSe at ambient pressure introduced in Ref. [25], and H_U is the first-principles multiorbital interaction for FeSe [42]. In FeSe, $\bar{U} = 7.21\text{eV}$ and $\bar{J} = 0.68\text{eV}$ on average. Here, r is the reduction factor for the interaction term [25]. We denote $d_{z^2}, d_{xz}, d_{yz}, d_{xy}, d_{x^2-y^2}$ orbitals as 1, 2, 3, 4, 5, and p_x, p_y, p_z orbitals as 6, 7, 8. We introduce the renormalization factor $z_4 = 1/1.2$ and $z_l = 1$ for $l \neq 4$ [25], consistently with the microscopic theory in Ref. [43].

In Eq. (1), H_P represents the change in the kinetic term under pressure. To derive H_P , we perform the band calculation using the crystal structure of FeSe under pressure [44, 45]: The most dominant pressure-induced change is the lift of the xy -orbital level around $\mathbf{q} = (\pi, \pi)$ due to the increase of the Se-atom height [46, 47]. To shift the E_{xy} -level by ΔE_{xy} at $\mathbf{q} = (\pi, \pi)$, we set $H_P = \sum_{i,j,\sigma} \delta t_{i,j} c_{i,4\sigma}^\dagger c_{j,4\sigma}$, where $\delta t_{i,j} = \Delta E_{xy}/4$ for the on-site ($i = j$), $\delta t_{i,j} = -\Delta E_{xy}/8$ and $\delta t_{i,j} = \Delta E_{xy}/16$ for the first- and second-nearest sites [25]; see the Supplemental Material (SM):A [48]. Figure 1 (a) shows the bandstructure for $\Delta E_{xy} = 0, 0.06$, and 0.12 eV, given by the solutions of $\det\{\hat{Z} \cdot \epsilon - (\hat{H}_0(\mathbf{k}) + \hat{H}_P(\mathbf{k}))\} = 0$, or equivalently given by the eigenvalues of $\hat{Z}^{-1/2}(\hat{H}_0(\mathbf{k}) + \hat{H}_P(\mathbf{k}))\hat{Z}^{-1/2}$, where $Z_{l,m} = (1/z_l)\delta_{l,m}$ [25, 26].

The Fermi surfaces (FSs) for $\Delta E_{xy} = 0$ and 0.12 eV are shown in Figs. 1 (b) and (c), respectively. In the present model, xy -orbital pocket appear for $\Delta E_{xy} \gtrsim 0.1\text{eV}$. According to the first principles study, $\Delta E_{xy} \sim 0.1\text{eV}$ is realized under ~ 4 GPa [48]. In FeSe at ambient pressure, the top of the xy -hole pocket is about 40meV below the Fermi level experimentally [20], which corresponds to $\Delta E_{xy} \sim 0.05\text{eV}$ in the present model.

Hereafter, we analyze the model Hamiltonian (1) based on the self-consistent VC (SC-VC) theory. The spin- or charge-channel susceptibility is given as

$$\hat{\chi}^x(q) = \hat{\Phi}^x(q)[1 - \hat{U}^{0x}\hat{\Phi}^x(q)]^{-1} \quad (x = s, c), \quad (2)$$

where $x = s$ or c , and $q = (\omega_l = 2\pi lT, \mathbf{q})$. \hat{U}^{0x} is the first-principles Coulomb interaction for FeSe derived in Ref. [42], and it was introduced as $\hat{\Gamma}^x$ in Ref. [25]. The irreducible susceptibility is $\hat{\Phi}^x(q) = \hat{\chi}^0(q) + \hat{X}^x(q)$, where $\hat{\chi}^0(q)$ is the bare susceptibility and $\hat{X}^x(q)$ is the VC that is dropped in the random-phase-approximation (RPA). The spin (charge) Stoner factor $\alpha_{S(C)}$ is defined as the largest eigenvalue of $\hat{U}^{0s(c)}\hat{\Phi}^{s(c)}(q)$: The magnetic order (orbital order) is established when $\alpha_{S(C)} = 1$.

In the SC-VC theory, we calculate both the Maki-Thompson-type VC and the AL-type VC, which are the first-order and the second-order diagrams with respect to χ^x , respectively [10, 25]. Figure 2 (a) shows the diagrammatic expression for the AL-type VC $X_{yz}^c(\mathbf{0}) \sim$

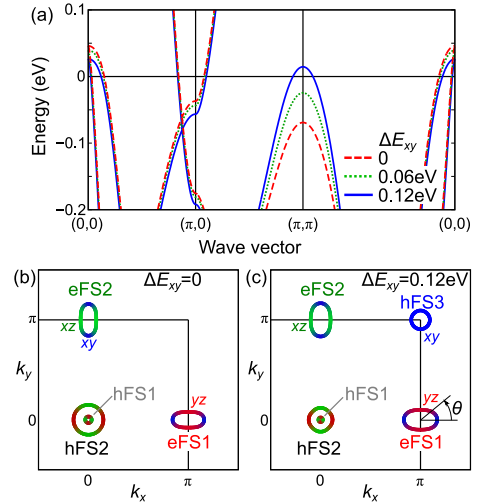


FIG. 1: (color online) (a) Band structure of the present FeSe model for $\Delta E_{xy} = 0, 0.06$ and 0.12 eV. (b) FSs for $\Delta E_{xy} = 0$ and (c) FSs for $\Delta E_{xy} = 0.12\text{eV}$. The hFS3 is the xy -orbital hole-pocket. The colors green, red, and blue represents the xz, yz , and xy orbitals, respectively.

$|\Lambda_{yz}^0|^2 T \sum_{\mathbf{q}} \{\chi_{yz}^s(\mathbf{q})\}^2$. Here, $\hat{\Lambda}_{yz}^0$ is the three-point vertex for yz -orbital, given by $\hat{\Lambda}_{3,3,3,3,3,3}^0(\mathbf{0}; \mathbf{Q})$ in Fig. 2 (b) [10]. Thus, $X_{yz}^c(\mathbf{0})$ increases in proportion to $\sum_{\mathbf{q}} \{\chi_{yz}^s(\mathbf{q})\}^2 \sim \chi_{yz}^s(\mathbf{Q})$. The increment of the AL-VC drives the strong nematic orbital susceptibility for $O = n_{xz} - n_{yz}$, $\chi^{\text{orb}}(\mathbf{0}) \equiv \sum_{l,m}^{2,3} (-1)^{l+m} \chi_{l,l,m,m}^c(\mathbf{0})$. Here, we calculate only the charge-channel VC $X_{l,l',m,m'}^c(q)$ for $l, l', m, m' = 2 \sim 4$ except for $l = l' = m = m' = 4$, by following Ref. [10], which is justified for various Fe-based superconductors [10, 25]. In the SM:B [48], we explain that essentially similar results are obtained if we perform the self-consistent calculation for both $\hat{X}^s(q)$ and $\hat{X}^c(q)$ for all d -orbitals.

In Fig. 2 (c), we show the spin susceptibility on xy -orbital, $\chi_{xy}^s(\mathbf{q}) \equiv \chi_{4,4,4,4}^s(\mathbf{q})$, at $r = 0.266$ and $T = 30\text{meV}$. For $\Delta E_{xy} = 0.12\text{eV}$, the hFS3 at (π, π) appears, and therefore $\chi_{xy}^s(\mathbf{Q})$ ($\mathbf{Q} = (\pi, 0)$) is drastically enlarged due to the good nesting between eFS1,2 and the hFS3 on xy -orbital. We stress that the emergence of the hFS3 could lead to the inhomogeneous phase separation as discussed in Ref. [49]. In contrast, $\chi_{yz}^s(\mathbf{q}) \equiv \chi_{3,3,3,3}^s(\mathbf{q})$ in Fig. 2 (d) gently decreases with ΔE_{xy} , since the nesting condition on yz -orbital becomes worse due to the shrinkage (expansion) of hFS1,2 (eFS1,2). This suppression of $\chi_{yz}^s(\mathbf{Q})$ caused the reduction of the orbital susceptibility in Fig. 2 (e), due to the reduction of the AL-term $X_{yz}^c(\mathbf{0}) \propto \chi_{yz}^s(\mathbf{Q})$. Such drastic ΔE_{xy} -dependences of the spin and orbital susceptibilities are contributed by the smallness of the FSs in FeSe.

Figure 2 (f) shows the Stoner factors $\alpha_{S,C}$ obtained by the SC-VC theory for $r = 0.266$ at $T = 30\text{meV}$. The obtained $\alpha_{S(C)}$ is qualitatively proportional to $T_{m(\text{str})}$. At $\Delta E_{xy} = 0$, which corresponds to $P = 0\text{GPa}$, α_C is

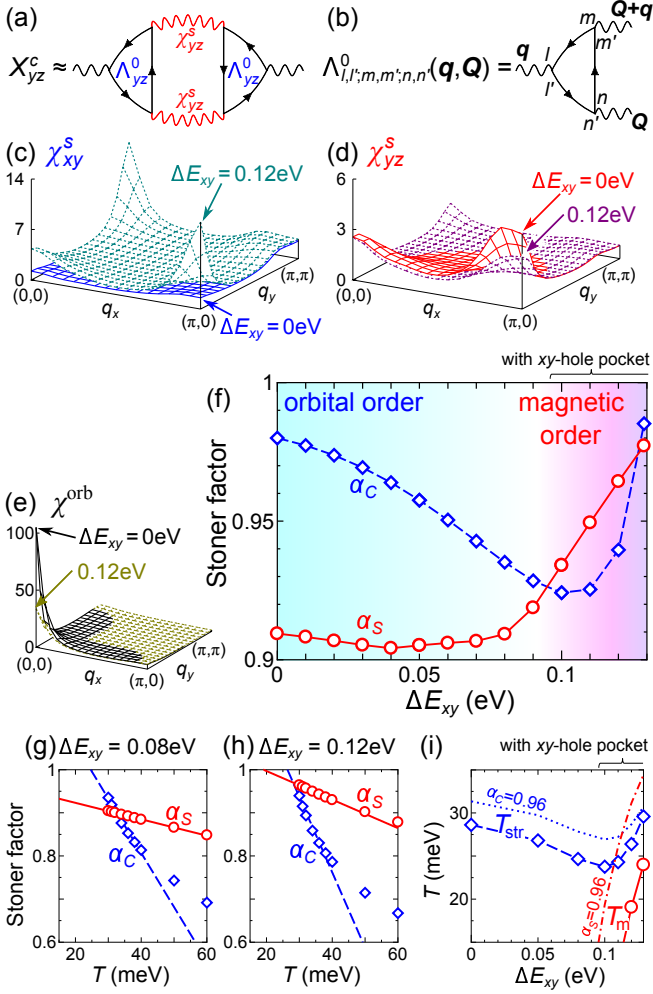


FIG. 2: (color online) (a) Charge-channel AL-type VC for the yz -orbital and (b) three-point vertex. (c) $\chi_{xy}^s(\mathbf{q})$, (d) $\chi_{yz}^s(\mathbf{q})$, and (e) $\chi^{\text{orb}}(\mathbf{q})$ or $\Delta E_{xy} = 0$ and 0.12 eV at $r = 0.266$ and $T = 30$ meV. (f) Stoner factors as functions of ΔE_{xy} at $r = 0.266$ and $T = 30$ meV. (g) T -dependences of $\alpha_{S,C}$ for $\Delta E_{xy} = 0.08$ eV and (h) those for $\Delta E_{xy} = 0.12$ eV. (i) T_m and T_{str} defined by the relation $\alpha_{S,C} = 1$ and 0.96 .

close to the unity whereas $\alpha_S \sim 0.9$. When $\Delta E_{xy} > 0$, the chemical potential μ increases even for $\Delta E_{xy} \ll 0.1$ eV due to the finite- T effect. Then, the nesting between hFS1,2 and eFS1 becomes worse, and therefore $\chi_{yz}^s(\mathbf{Q})$ gradually decreases. At the same time, α_C decreases since $X_{yz}^c(\mathbf{0}) \sim |\Lambda_{yz}^0|^2 T \sum_{\mathbf{q}} \{\chi_{yz}^s(\mathbf{q})\}^2$ becomes smaller, consistently with the experimental reduction of T_{str} under $P = 0 \sim 2$ GPa. In contrast, $\chi_{xy}^s(\mathbf{Q})$ starts to increase for $\Delta E_{xy} \gtrsim 0.08$ eV, due to the nesting between the hFS3 and eFS1,2 on xy -orbital. For this reason, α_S rapidly increases in Fig. 2 (f). When $\Delta E_{xy} \gtrsim 0.1$ eV, α_C starts to increase since $\chi_{xy}^s(\mathbf{q})$ also contribute to the “AL-term on yz -orbital through $|\Lambda_{yz-xy}^0|^2 T \sum_{\mathbf{q}} \chi_{xy}^s(\mathbf{q})^2$ ”, where $\Lambda_{yz-xy}^0 \equiv \Lambda_{3,3;4,4;4,4}^0(\mathbf{0}; \mathbf{Q})$. Although the off-diagonal three-point vertex Λ_{yz-xy}^0 is much smaller than

the diagonal one Λ_{yz}^0 , it is finite since the electron-FSS are composed of three orbitals 2 ~ 4.

To confirm the validity of the simplified pressure term H_P introduced in the present study, we derive the pressure term from the first principles study, H_P^{1st} , and perform the numerical study based on the SC-VC theory in the SM: D [48]. The obtained P -dependences of α_S and α_C are consistent with Fig. 2 (f).

We also estimate the transition temperatures T_m and T_{str} . As shown in Figs. 2 (g) and (h), the Stoner factors $\alpha_{S(C)}$ follow the T -linear relations for $T \gtrsim 30$ meV, at $\Delta E_{xy} = 0.08$ eV and 0.12 eV. (Then, $\chi^s(\mathbf{Q})$ and $\chi^{\text{orb}}(\mathbf{0})$ follow the Curie-Weiss relations.) By extrapolating the T -linear relations, we estimate T_m and T_{str} under the condition $\alpha_{S,C} = 1$ and $\alpha_{S,C} = 0.96$ in Fig. 2 (i). In both cases, T_{str} decreases with ΔE_{xy} for $\Delta E_{xy} < 0.1$ eV, whereas T_m drastically increases for $\Delta E_{xy} > 0.1$ eV, consistently with experimental phase diagram. In the region $T_m > T > T_{\text{str}}$ for $\alpha_{S,C} = 0.96$ with $\Delta E_{xy} > 0.11$ eV, the tetragonal (C_4) stripe magnetic phase appears, if the spin-lattice coupling is negligibly small.

In the next stage, we study the superconducting state. Both the spin [46, 50–53] and/or orbital [38, 54, 55] fluctuation mediated mechanisms have been studied. The linearized gap equation is

$$\lambda \Delta_{\alpha}(k) = -T \sum_{p, \beta} V_{\alpha, \beta}^{\text{SC}}(k, p) |G_{\beta}(p)|^2 \Delta_{\beta}(p), \quad (3)$$

where $k = ((2n+1)\pi T, \mathbf{k})$, $\Delta_{\alpha}(k)$ is the gap function on the α -FS, and λ is the eigenvalue that reaches unity at $T = T_c$. $V_{\alpha, \beta}^{\text{SC}}$ is the pairing interaction. In the conventional Migdal approximation, \hat{V}^{SC} in the orbital basis is given as $\hat{V}_{\text{Migdal}}(k, p) = \frac{3}{2} \hat{I}^s(k-p) + \frac{1}{2} \hat{I}^c(k-p) - \hat{U}^{0s}$, where $\hat{I}^x(q) = \hat{U}^{0x} + \hat{U}^{0x} \hat{\chi}^x(q) \hat{U}^{0x}$ ($x = s, c$). It is schematically shown in Fig. 3 (a). However, since this approximation is not justified for Fe-based superconductors, we introduce the following “beyond-Migdal-Eliashberg pairing interaction” introduced in Ref. [55]:

$$\hat{V}^{\text{tot}}(k, p) = \hat{V}^{\Lambda}(k, p) + \hat{V}^{\text{cross}}(k, p), \quad (4)$$

which are depicted in Figs. 3 (b) and (c). $\hat{\Lambda}^x$ in Fig. 3 (b) is the VC for the coupling constant \hat{U}^{0x} , called the U -VC. Since $|\Lambda^c|^2 \gg 1$ due to the AL-type VC shown in Fig. 3 (d) [55, 56], moderate orbital fluctuations give sizable attractive interaction. Also, V^{cross} is the “AL-type crossing fluctuation interaction” [55]. The analytic expressions for Figs. 3 (b)-(d) are explained in Refs. [55, 56] and in the SM: E [48]. In Ref. [56], we verified the significance of the U -VC by applying the functional-renormalization-group (fRG) method to the two-orbital Hubbard model. The fRG method enables us to generate the higher-order VCs (including the higher-order processes other than Figs. 3 (a)-(d)) in a systematic and unbiased way.

The eigenvalue λ^{tot} obtained for V^{tot} in the absence of the nematicity and magnetism is shown in Fig. 3 (e),

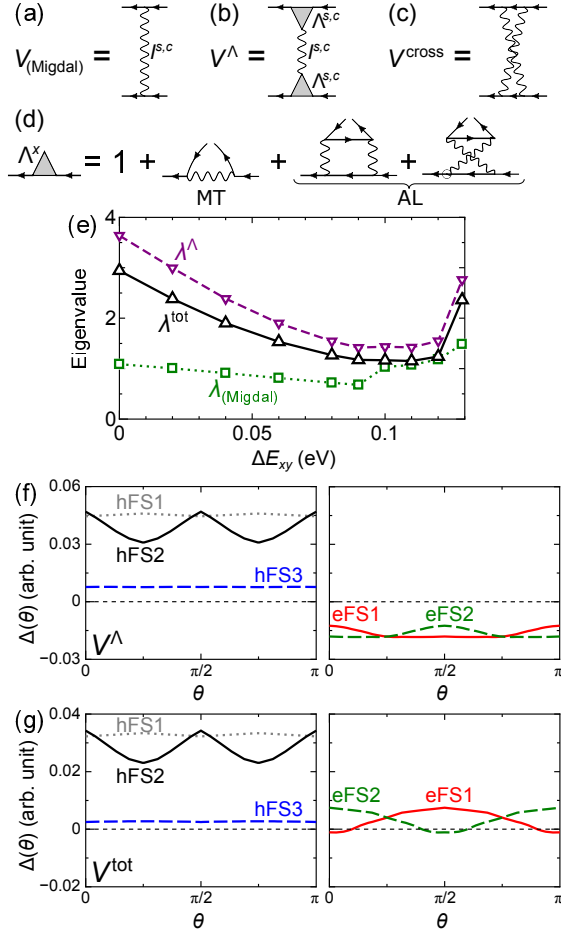


FIG. 3: (color online) (a) V_{Migdal} , (b) V^Λ , and (c) V^{cross} . (d) U - VC Λ^x . (e) Eigenvalues for various pairing interactions: λ^{tot} for V^{tot} , λ^Λ for V^Λ , and λ_{Migdal} for V_{Migdal} . (f) s_{\pm} -wave gap given by V^Λ for $\Delta E_{xy} = 0.12\text{eV}$. (g) s_{++} -wave gap given by V^{tot} . The FSs are shown in Fig. 1 (c). Numerical study is performed in the nonmagnetic state.

together with λ_{Migdal} for V_{Migdal} and λ^Λ for V^Λ : The relation $\lambda_{\text{Migdal}} \ll \lambda^\Lambda$ means that the charge U - VC strongly enlarges T_c . For $V^{\text{SC}} = V^\Lambda$ at $\Delta E_{xy} = 0.12\text{eV}$, the s_{\pm} -wave state with sign reversal between electron- and hole-pockets is obtained as shown in Fig. 3 (f). In contrast, the “ s_{++} -wave state without sign reversal” is obtained for the total pairing interaction V^{tot} , since V^{cross} gives large inter-pocket attractive interaction: The obtained nodal s_{++} -wave state at $\Delta E_{xy} = 0.12\text{eV}$ is shown in Fig. 3 (g). The s_{++} -state will be stabilized by the pressure-induced strong e - ph interaction [47].

Finally, we study the superconductivity in FeSe in the nematic state at $P = 0$ [57]. Figure 4 (a) shows the FSs and bandstructure under the sign-reversing orbital polarization reported in Ref. [20]: We set $\delta E_{\text{nem}} \equiv E_{yz} - E_{xz} = -30\text{meV}$ at Γ point, and $\delta E_{\text{nem}} = 60\text{meV}$ at X and Y points by following Ref. [25]. The susceptibilities obtained by the SC-VC theory for $z_4^{-1} = 1.2$ and $r =$

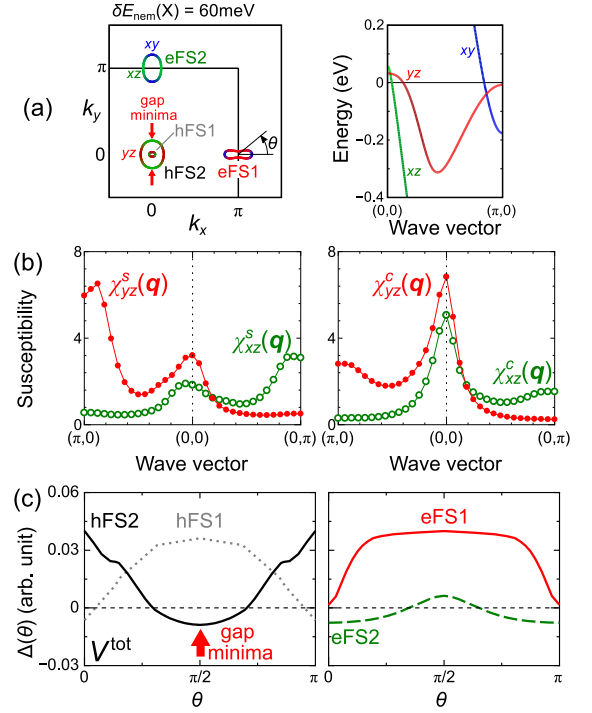


FIG. 4: (color online) (a) FSs and bandstructure in the presence of the sign-reversing orbital polarization $\delta E_{\text{nem}}(\Gamma) = -30\text{meV}$ and $\delta E_{\text{nem}}(X) = 60\text{meV}$. Here, $\Delta E_{xy} = 0$. (b) $\chi_{xz}^s(\mathbf{q})$, $\chi_{yz}^s(\mathbf{q})$, $\chi_{xz}^c(\mathbf{q})$, and $\chi_{yz}^c(\mathbf{q})$ obtained by the SC-VC theory. (c) s -wave gap functions obtained for V^{tot} : The gap functions on each FS is nodal.

0.266 at $T = 30\text{meV}$ [$(\alpha_S, \alpha_C) = (0.914, 0.934)$] are shown in Fig. 4 (b). By introducing δE_{nem} , $\chi_{yz}^s(\pi, 0)$ increases whereas $\chi_{xz}^s(0, \pi)$ decreases as explained in Ref. [54]. Then, the AL-term $X_{yz}^c(\mathbf{q})$ is enlarged due to the large $\chi_{yz}^s(\pi, 0)$. The obtained strong ferro- and antiferro-orbital fluctuations give significant pairing interaction on the yz -orbital.

Figure 4 (c) shows the s -wave gap function obtained for V^{tot} . Here, the gap is large on the FSs with large yz -orbital component, since strong intra-pocket force and inter-pocket attractive one are caused by large $\chi_{yz}^c(\mathbf{q})$ at $\mathbf{q} \sim \mathbf{0}$ and $\mathbf{q} \sim (\pi, 0)$ in addition to V^{cross} . The position of the nodal part on hole-FS is consistent with the experimental report [41]. The nodal structure on Δ_{hFS} is unchanged when two Dirac cones appear near X-point for larger $\delta E_{\text{nem}}(X)$, as we show in SM: C [48]. Thus, the nodal gap structure is robust against model parameters, whereas the ratio between $|\Delta_{\text{hFS}}|$ and $|\Delta_{\text{eFS}}|$ is sensitive to parameters, so it is our future problem to explain the experimental data quantitatively.

In summary, we studied the electronic states in FeSe at ambient pressure and under pressure. We predicted that the hFS3 appears under pressure. Due to this pressure-induced Lifshitz transition, the spin fluctuations on the xy orbital are enlarged, whereas those on the xz, yz orbitals are reduced gently. Since the orbital order is driven

by the spin fluctuations on xz, yz orbitals via the intra-orbital VCs, the nematicity is suppressed and replaced with the magnetism on the xy orbital electrons under pressure. Also, both the nodal s -wave state in the nematic state at ambient pressure and the enlargement of T_c under pressure are satisfactorily explained, due to the novel cooperation between spin and orbital fluctuations.

We are grateful to A. Chubukov, P.J. Hirschfeld, R. Fernandes, J. Schmalian, D.L. Feng, S. Shin, Y. Matsuda, T. Shibauchi, K. Okazaki and T. Shimojima for useful discussions. This study has been supported by Grants-in-Aid for Scientific Research from MEXT of Japan.

-
- [1] M. Yoshizawa, D. Kimura, T. Chiba, S. Simayi, Y. Nakanishi, K. Kihou, C.-H. Lee, A. Iyo, H. Eisaki, M. Nakajima, and S. Uchida, *J. Phys. Soc. Jpn.* **81**, 024604 (2012).
- [2] J. L. Niedziela, D. Parshall, K. A. Lokshin, A. S. Sefat, A. Alatas, and T. Egami, *Phys. Rev. B* **84**, 224305 (2011).
- [3] Y. Gallais, R. M. Fernandes, I. Paul, L. Chauvière, Y.-X. Yang, M.-A. Méasson, M. Cazayous, A. Sacuto, D. Colson, and A. Forget, *Phys. Rev. Lett.* **111**, 267001 (2013).
- [4] M. Yi, D. Lu, J.-H. Chu, J. G. Analytis, A. P. Sorini, A. F. Kemper, B. Moritz, S.-K. Mo, R. G. Moore, M. Hashimoto, W.-S. Lee, Z. Hussain, T. P. Devereaux, I. R. Fisher, and Z.-X. Shen, *Proc. Natl. Acad. Sci. USA* **108**, 6878 (2011).
- [5] C. Fang, H. Yao, W.-F. Tsai, J. P. Hu, and S. A. Kivelson, *Phys. Rev. B* **77**, 224509 (2008).
- [6] R. M. Fernandes, L. H. VanBebber, S. Bhattacharya, P. Chandra, V. Keppens, D. Mandrus, M. A. McGuire, B. C. Sales, A. S. Sefat, and J. Schmalian, *Phys. Rev. Lett.* **105**, 157003 (2010).
- [7] R. M. Fernandes, A. V. Chubukov, J. Knolle, I. Eremin, and J. Schmalian, *Phys. Rev. B* **85**, 024534 (2012).
- [8] F. Krüger, S. Kumar, J. Zaanen, and J. van den Brink, *Phys. Rev. B* **79**, 054504 (2009).
- [9] C.-C. Lee, W.-G. Yin, and W. Ku, *Phys. Rev. Lett.* **103**, 267001 (2009).
- [10] S. Onari and H. Kontani, *Phys. Rev. Lett.* **109**, 137001 (2012).
- [11] S.-H. Baek, D. V. Efremov, J. M. Ok, J. S. Kim, J. van den Brink, and B. Büchner, *Nat. Mater.* **14**, 210 (2015).
- [12] A. E. Böhmer, T. Arai, F. Hardy, T. Hattori, T. Iye, T. Wolf, H. v. Löhneysen, K. Ishida, and C. Meingast, *Phys. Rev. Lett.* **114**, 027001 (2015).
- [13] P. Massat, D. Farina, I. Paul, S. Karlsson, P. Strobel, P. Toulemonde, M.-A. Méasson, M. Cazayous, A. Sacuto, S. Kasahara, T. Shibauchi, Y. Matsuda, and Y. Gallais, *Proc. Natl. Acad. Sci. USA* **113**, 9177 (2016).
- [14] S. Hosoi, K. Matsuura, K. Ishida, H. Wang, Y. Mizukami, T. Watashige, S. Kasahara, Y. Matsuda, and T. Shibauchi, *Proc. Natl. Acad. Sci. USA* **113**, 8139 (2016).
- [15] K. Nakayama, Y. Miyata, G. N. Phan, T. Sato, Y. Tanabe, T. Urata, K. Tanigaki, and T. Takahashi, *Phys. Rev. Lett.* **113**, 237001 (2014).
- [16] M. D. Watson, T. K. Kim, A. A. Haghighirad, N. R. Davies, A. McCollam, A. Narayanan, S. F. Blake, Y. L. Chen, S. Ghannadzadeh, A. J. Schofield, M. Hoesch, C. Meingast, T. Wolf, and A. I. Coldea, *Phys. Rev. B* **91**, 155106 (2015).
- [17] T. Shimojima, Y. Suzuki, T. Sonobe, A. Nakamura, M. Sakano, J. Omachi, K. Yoshioka, M. Kuwata-Gonokami, K. Ono, H. Kumigashira, A. E. Böhmer, F. Hardy, T. Wolf, C. Meingast, H. v. Löhneysen, H. Ikeda, and K. Ishizaka, *Phys. Rev. B* **90**, 121111(R) (2014).
- [18] P. Zhang, T. Qian, P. Richard, X. P. Wang, H. Miao, B. Q. Lv, B. B. Fu, T. Wolf, C. Meingast, X. X. Wu, Z. Q. Wang, J. P. Hu, and H. Ding, *Phys. Rev. B* **91**, 214503 (2015).
- [19] Y. Zhang, M. Yi, Z.-K. Liu, W. Li, J. J. Lee, R. G. Moore, M. Hashimoto, N. Masamichi, H. Eisaki, S.-K. Mo, Z. Hussain, T. P. Devereaux, Z.-X. Shen, and D. H. Lu, *Phys. Rev. B* **94**, 115153 (2016).
- [20] Y. Suzuki, T. Shimojima, T. Sonobe, A. Nakamura, M. Sakano, H. Tsuji, J. Omachi, K. Yoshioka, M. Kuwata-Gonokami, T. Watashige, R. Kobayashi, S. Kasahara, T. Shibauchi, Y. Matsuda, Y. Yamakawa, H. Kontani, and K. Ishizaka, *Phys. Rev. B* **92**, 205117 (2015).
- [21] J. K. Glasbrenner, I. I. Mazin, H. O. Jeschke, P. J. Hirschfeld, R. M. Fernandes, and R. Valentí, *Nat. Phys.* **11**, 953 (2015).
- [22] F. Wang, S. A. Kivelson, and D.-H. Lee, *Nat Phys* **11**, 959 (2015).
- [23] R. Yu and Q. Si, *Phys. Rev. Lett.* **115**, 116401 (2015).
- [24] L. Fanfarillo, A. Cortijo, and B. Valenzuela, *Phys. Rev. B* **91**, 214515 (2015).
- [25] Y. Yamakawa, S. Onari, and H. Kontani, *Phys. Rev. X* **6**, 021032 (2016).
- [26] S. Onari, Y. Yamakawa, and H. Kontani, *Phys. Rev. Lett.* **116**, 227001 (2016).
- [27] A. V. Chubukov, M. Khodas, and R. M. Fernandes, arXiv:1602.05503.
- [28] K. Jiang, J. Hu, H. Ding, and Z. Wang, *Phys. Rev. B* **93**, 115138 (2016).
- [29] L. Fanfarillo, G. Giovannetti, M. Capone, and E. Bascones, *Phys. Rev. B* **95**, 144511 (2017).
- [30] T. Imai, K. Ahilan, F. L. Ning, T. M. McQueen, and R. J. Cava, *Phys. Rev. Lett.* **102**, 177005 (2009).
- [31] Y. Mizuguchi and Y. Takano, *J. Phys. Soc. Jpn.* **79**, 102001 (2010).
- [32] M. Bendele, A. Amato, K. Conder, M. Elender, H. Keller, H.-H. Klauss, H. Luetkens, E. Pomjakushina, A. Raselli, and R. Khasanov, *Phys. Rev. Lett.* **104**, 087003 (2010).
- [33] M. Bendele, A. Ichsanow, Y. Pashkevich, L. Keller, T. Strässle, A. Gusev, E. Pomjakushina, K. Conder, R. Khasanov, and H. Keller, *Phys. Rev. B* **85**, 064517 (2012).
- [34] T. Terashima, N. Kikugawa, S. Kasahara, T. Watashige, T. Shibauchi, Y. Matsuda, T. Wolf, A. E. Böhmer, F. Hardy, C. Meingast, H. v. Löhneysen, and S. Uji, *J. Phys. Soc. Jpn.* **84**, 063701 (2015).
- [35] K. Kothapalli, A. E. Böhmer, W. T. Jayasekara, B. G. Ueland, P. Das, A. Sapkota, V. Taufour, Y. Xiao, E. Alp, S. L. Bud'ko, P. C. Canfield, A. Kreyssig, and A. I. Goldman, *Nat. Commun.* **7**, 12728 (2016).
- [36] P. Wang, S. Sun, Y. Cui, W. Song, T. Li, R. Yu, H. Lei, and W. Yu, *Phys. Rev. Lett.* **117**, 237001 (2016).
- [37] J. P. Sun, K. Matsuura, G. Z. Ye, Y. Mizukami, M. Shimozawa, K. Matsubayashi, M. Yamashita, T. Watashige, S. Kasahara, Y. Matsuda, J.-Q. Yan, B. C. Sales, Y. Uwatoko, J.-G. Cheng, and T. Shibauchi, *Nat. Commun.* **7**,

- 12146 (2016).
- [38] S. Onari, Y. Yamakawa, and H. Kontani, *Phys. Rev. Lett.* **112**, 187001 (2014).
 - [39] C.-L. Song, Y.-L. Wang, P. Cheng, Y.-P. Jiang, W. Li, T. Zhang, Z. Li, K. He, L. Wang, J.-F. Jia, H.-H. Hung, C. Wu, X. Ma, X. Chen, and Q.-K. Xue, *Science* **332**, 1410 (2011).
 - [40] S. Kasahara, T. Watashige, T. Hanaguri, Y. Kohsaka, T. Yamashita, Y. Shimoyama, Y. Mizukami, R. Endo, H. Ikeda, K. Aoyama, T. Terashima, S. Uji, T. Wolf, H. von Löhneysen, T. Shibauchi, and Y. Matsuda, *Proc. Natl. Acad. Sci. USA* **111**, 16309 (2014).
 - [41] H. C. Xu, X. H. Niu, D. F. Xu, J. Jiang, Q. Yao, M. Abdel-Hafiez, D. A. Chareev, A. N. Vasiliev, R. Peng, and D. L. Feng, *Phys. Rev. Lett.* **117**, 157003 (2016).
 - [42] T. Miyake, K. Nakamura, R. Arita, and M. Imada, *J. Phys. Soc. Jpn.* **79**, 044705 (2010).
 - [43] Z. P. Yin, K. Haule, and G. Kotliar, *Nat. Mater.* **10**, 932 (2011).
 - [44] J. N. Millican, D. Phelan, E. L. Thomas, J. B. Leão, and E. Carpenter, *Solid State Commun.* **149**, 707 (2009).
 - [45] A. E. Böhrer, F. Hardy, F. Eilers, D. Ernst, P. Adelmann, P. Schweiss, T. Wolf, and C. Meingast, *Phys. Rev. B* **87**, 180505(R) (2013).
 - [46] K. Kuroki, H. Usui, S. Onari, R. Arita, and H. Aoki, *Phys. Rev. B* **79**, 224511 (2009).
 - [47] S. Mandal, R. E. Cohen and K. Haule, *Phys. Rev. B* **89**, 220502(R) (2014).
 - [48] Supplemental Material.
 - [49] A. O. Sboychakov, A. V. Rozhkov, K. I. Kugel, A. L. Rakhmanov, and F. Nori, *Phys. Rev. B* **88**, 195142 (2013).
 - [50] I. I. Mazin, D. J. Singh, M. D. Johannes, and M. H. Du, *Phys. Rev. Lett.* **101**, 057003 (2008).
 - [51] A. V. Chubukov, D. V. Efremov, and I. Eremin, *Phys. Rev. B* **78**, 134512 (2008).
 - [52] S. Graser, G. R. Boyd, C. Cao, H.-P. Cheng, P. J. Hirschfeld, and D. J. Scalapino, *Phys. Rev. B* **77**, 180514(R) (2008).
 - [53] A. Chubukov and P. J. Hirschfeld, *Physics Today* **68**, 46 (2015).
 - [54] H. Kontani, T. Saito, and S. Onari, *Phys. Rev. B* **84**, 024528 (2011).
 - [55] Y. Yamakawa, and H. Kontani, arXiv:1611.05375.
 - [56] R. Tazai, Y. Yamakawa, M. Tsuchiizu, and H. Kontani, *Phys. Rev. B* **94**, 115155 (2016).
 - [57] S. Mukherjee, A. Kreisel, P. J. Hirschfeld, and B. M. Andersen, *Phys. Rev. Lett.* **115**, 026402 (2015): The authors studied the gap equation for FeSe model with the constant orbital polarization using the RPA. The obtained gap on the hole-pocket is fully-gapped.

[Supplementary Material]

Nematicity, magnetism and superconductivity in FeSe under pressure:
Unified explanation based on the self-consistent vertex correction theory

Youchi Yamakawa, Hiroshi Kontani

A: First principles model Hamiltonian

In the main text, we studied the electronic states in FeSe under pressure by using the SC-VC theory. To describe the change in the bandstructure under pressure, we introduced the additional term H_P into the model Hamiltonian for FeSe at ambient pressure. We set $H_P = \sum_{i,j,\sigma} \delta t_{i,j} c_{i,4\sigma}^\dagger c_{j,4\sigma}$, where $\delta t_{i,j} = \Delta E_{xy}/4$ for the on-site ($i = j$), $\delta t_{i,j} = -\Delta E_{xy}/8$ and $\delta t_{i,j} = \Delta E_{xy}/16$ for the first- and second-nearest sites. By introducing H_P , the d_{xy} -orbital level around (π, π) is lifted by ΔE_{xy} .

To justify the validity of H_P , we perform the band calculation by using the WIEN2k code. We use the crystal structure of FeSe under pressure reported in Ref. [1] for $0 \sim 0.6$ GPa, which are shown in Fig. S1 (a). We perform the first principles calculation using the WIEN2k code for $P = 0$ GPa and 0.6 GPa, and find that E_{xy} -level at Γ -point is lifted by 13 meV, whereas $E_{xz(yz)}$ -level at Γ -point is lowered by 9 meV by applying 0.6 GPa. That is, the difference $E_{xy} - E_{xz(yz)}$ increases by 25 meV by applying 0.6 GPa. This result is consistent with the theoretical report in Ref. [3] that the top of the d_{xy} -orbital hole-pocket is lifted as increasing z_{Se} .

According to the recent study for FeSe under high pressure [4], the lattice constants a and c linearly decrease in proportion to P for $P < 4$ GPa. Here, we perform the band calculations for $P = 0$ GPa and 4 GPa, by assuming the linear extrapolations of a , b and z_{Se} from Fig. S1 (a). The dispersion on the $k_z = 0$ plane in the three-dimensional WIEN2k bandstructure are shown in Fig. S1 (b). It is predicted that $E_{xy} - E_{xz(yz)}$ increases by 170 meV by applying 4 GPa. Similar orbital-dependent change in the bandstructure is obtained even if we drop the inter-layer hoppings, as we show in Fig. S5 (b). Therefore, it is natural to expect that the top of the d_{xy} -hole pocket, which is about 40 meV below the Fermi level at 0 GPa [5], is shifted to above the Fermi level under pressure. Thus, the simplified pressure term H_P in the main text is justified.

In the main text, we analyze the total Hamiltonian $H = H_0 + H_P + rH_U$, where H_0 is the kinetic term at $P = 0$ introduced in Ref. [6], and H_U is the screened Coulomb interaction due to the valence-bands obtained by the constraint-RPA (cRPA) method [7]. We neglect the pressure dependence of H_U since the screening would be insensitive to the pressure-induced change in the valence-band structure. Here, we introduce the

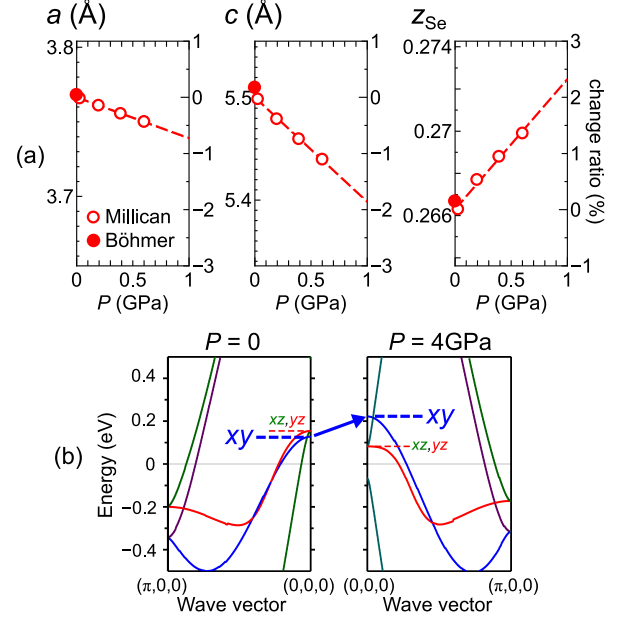


FIG. S1: (color online) (a) Crystal structure parameters a , b and z_{Se} for $P = 0 \sim 0.6$ GPa reported by Millican *et al* [1]. The Crystal structure parameters at ambient pressure reported in Ref. [2] are also shown. (b) Dispersions on the k_x - k_y plane in the three-dimensional WIEN2k bandstructure for $P = 0$ and $P = 4$ GPa. The characteristic change in the bandstructure is reproduced by introducing ΔE_{xy} , as shown in Fig. 1 (a) in the main text.

reduction factor r and the orbital-dependent renormalization factor z_l ($l = 1 \sim 5$). In the case of $z_l = z$ for all l , the Stoner factors for the parameters (r, T) at $z = 1$ are equal to those for $(r/z, zT)$ at $z < 1$. [6].

In this study, we put $z_4 < 1$ and $z_l = 1$ ($l \neq 4$), which is consistent with the experimental relation by ARPES. In the present numerical study at $T \leq 30$ meV, we put $1/z_4 = 1.2$ in order to reproduce the moderate spin fluctuations at $\mathbf{q} = (\pi, 0)$ in FeSe at ambient pressure. (When $z_4 = 1$, $\chi^s(\mathbf{q})$ has the maximum at $\mathbf{q} = (\pi, \pi)$ due to the nesting between eFS1 and eFS2 on xy -orbital.) At $T = 50$ meV, $1/z_4$ should be larger than 1.5 to satisfy the relation $\chi^s(\pi, 0) > \chi^s(\pi, \pi)$ [8]. The reason is that the hFS1,2 shrink at $T = 50$ meV due to the temperature-induced shift in the chemical potential, so $\chi_{yz}^s(\pi, 0)$ is relatively reduced. Note that the numerical results for $1/z_4 = 1.2$ at $T = 30$ meV are essentially similar to the results for $1/z_4 = 1.6$ at $T = 50$ meV.

B: Full self-consistent vertex correction analysis

In the main text, we analyzed the eight-orbital Hubbard model for FeSe by using the SC-VC theory. In this theory, the VC for the spin and charge irreducible susceptibilities, $\hat{X}^s(q)$ and $\hat{X}^c(q)$, are calculated self-consistently. For $\hat{X}^{s,c}(q)$, both the Maki-Thompson-type VC and the AL-type VC are analyzed [6, 8, 9]. In the main text, we drop $\hat{X}^s(q)$ and calculate only the charge-channel VC $X_{l,l',m,m'}^c(q)$ for $l, l', m, m' = 2 \sim 4$ except for $l = l' = m = m' = 4$, by following the simplification introduced in Ref. [9]. This simplification is justified for Fe-based superconductors as verified in our previous studies [6, 8],

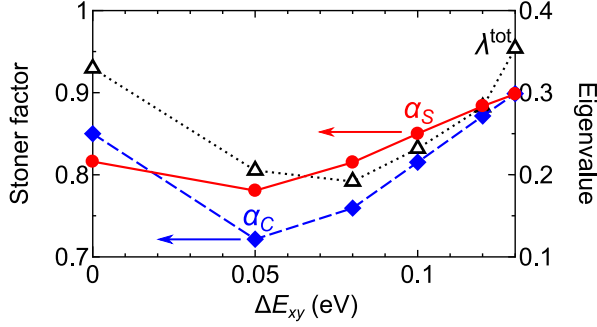


FIG. S2: (color online) Stoner factors (α_S, α_C) and gap equation eigenvalue for V^{tot} (λ^{tot}) as functions of ΔE_{xy} given by the full SC-VC analysis.

Here, we perform the time-consuming full self-consistent calculation for both $\hat{X}^s(q)$ and $\hat{X}^c(q)$ for all d -orbitals, in order to verify the validity of the numerical study in the main text. To reflect the increase of the bandwidth under pressure, we put $r = r_0 - a \cdot \Delta E_{xy}$, where $r_0 = 0.287$ and $a = 0.19$. Then, $r = 0.287$ (0.268) for $\Delta E_{xy} = 0$ (0.1) eV. In Fig. S2, we show the obtained Stoner factors α_S and α_C for $z_4^{-1} = 1.4$ at $T = 30\text{meV}$. For $\Delta E_{xy} = 0$, the obtained relation $\alpha_C > \alpha_S$ means that the orbital order is realized. When ΔE_{xy} increases to 0.05eV, both α_C and α_S decreases and the relation $\alpha_S > \alpha_C$ holds. For $\Delta E_{xy} > 0.05\text{eV}$, both α_C and α_S starts to increase, meaning that T_m increases with the pressure, consistently with the phase diagram in FeSe under pressure. In addition, we show the eigenvalue of the s -wave gap equation λ_{tot} obtained for V^{tot} . The increment of λ_{tot} for $\Delta E_{xy} > 0.08\text{eV}$ is consistent with the increment of T_c under pressure observed experimentally. In the present calculation, the intra-pocket attractive interaction is large whereas the interaction between hole- and electron-pockets is small because of the cancellation between attractive and repulsive interactions. For this reason, we find that both the s_{++} -wave and s_{\pm} -wave states can appear depending of the model parameters, and the impurity-induced $s_{\pm} \rightarrow s_{++}$ crossover is easily realized. Note that λ^{tot} in Fig. S2 is smaller than unity,

meaning that λ^{tot} given in the main text is overestimated due to the simplified analysis.

C: Gap functions for larger orbital polarization

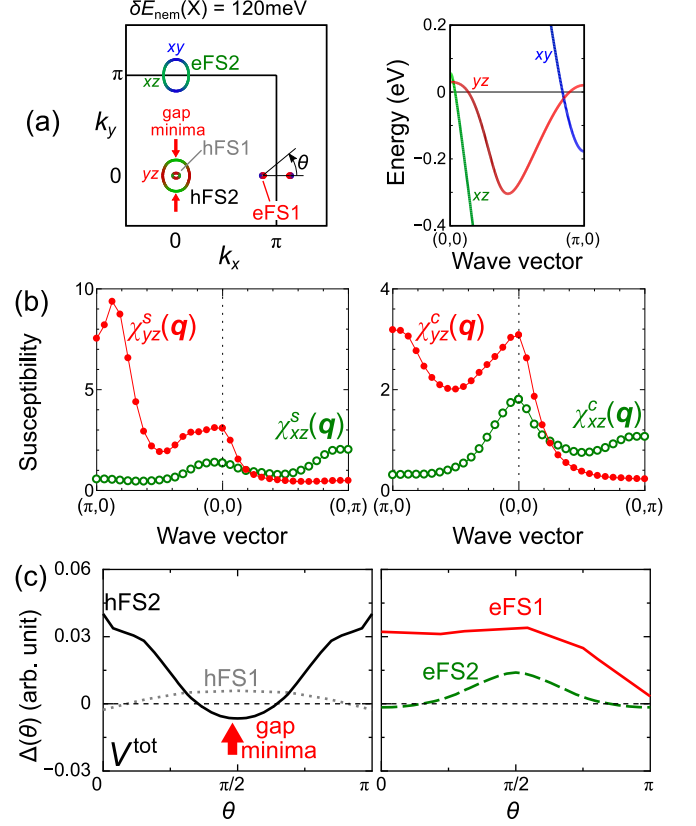


FIG. S3: (color online) (a) FSs and bandstructure for $\delta E_{\text{nem}}(\Gamma) = -30\text{meV}$ and $\delta E_{\text{nem}}(X) = 120\text{meV}$. Here, $\Delta E_{xy} = 0$. (b) $\chi_{xz}^s(q)$, $\chi_{yz}^s(q)$, $\chi_{xz}^c(q)$, and $\chi_{yz}^c(q)$ obtained by the SC-VC theory. (c) Gap functions obtained for V^{tot} ($\lambda^{\text{tot}} = 0.66$).

In the main text, we studied the gap function in FeSe for $\delta E_{\text{nem}}(X) = 60\text{meV}$, in which the horizontally-long electron-like FS is realized around the X-point. Here, we study the gap function for $\delta E_{\text{nem}}(X) > 100\text{meV}$, in which the electron-like FS is divided into two Dirac cones. We note that the experimentally observed orbital splitting is $z \cdot \delta E_{\text{nem}}$, where $z (\gtrsim 3)$ is the renormalization factor for xz, yz -orbitals [10].

First, we study the case $\delta E_{\text{nem}}(\Gamma) = -30\text{meV}$ and $\delta E_{\text{nem}}(X) = 120\text{meV}$. The FSs and bandstructure are shown in Fig. S3 (a): The Dirac cones around X-point are electron-like. The susceptibilities obtained by the SC-VC theory for $r = 0.266$ at $T = 30\text{meV}$ [$(\alpha_S, \alpha_C) = (0.953, 0.802)$] are shown in Fig. S3 (b). Here, we dropped the VC for the spin susceptibility as we did in the main text. Figure S3 (c) shows the s -wave gap function for $V^{\text{SC}} = V^{\text{tot}}$. Here, the gap is large

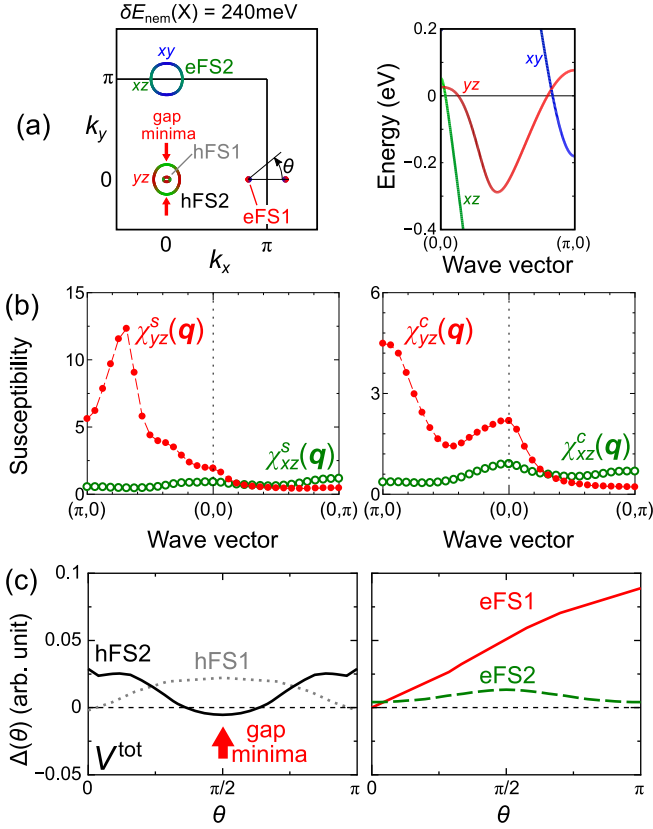


FIG. S4: (color online) (a) FSs and bandstructure for $\delta E_{\text{nem}}(\Gamma) = -30\text{meV}$ and $\delta E_{\text{nem}}(X) = 240\text{meV}$. (b) $\chi_{xz}^s(\mathbf{q})$, $\chi_{yz}^s(\mathbf{q})$, $\chi_{xz}^c(\mathbf{q})$, and $\chi_{yz}^c(\mathbf{q})$ obtained by the SC-VC theory. (c) Gap functions obtained for V^{tot} ($\lambda^{\text{tot}} = 0.79$).

on the FSs with large yz -orbital component, since large intra-pocket and inter-pocket attractive force are caused by large $\chi_{yz}^c(\mathbf{q})$ at $\mathbf{q} \sim \mathbf{0}$ and $\mathbf{q} \sim (\pi, 0)$. (We find that V^{cross} give weak repulsive interaction in this case.) The position of the nodal part on hole-FS is consistent with the experimental report [11].

Next, we study the case $\delta E_{\text{nem}}(\Gamma) = -30\text{meV}$ and $\delta E_{\text{nem}}(X) = 240\text{meV}$. The Dirac cones around X-point in Fig. S4 (a) are hole-like. The susceptibilities for $r = 0.266$ at $T = 30\text{ meV}$ [$(\alpha_S, \alpha_C) = (0.963, 0.842)$] are shown in Fig. S4 (b). Figure S4 (c) shows the s -wave gap function for $V^{\text{SC}} = V^{\text{tot}}$. In both cases, the gap function on the Dirac cone takes the largest value, which is consistent with the recent experimental report [12].

D: Numerical study based on H_P^{1st} given by the first-principles study

Here, we derive the pressure effect Hamiltonian $H_P^{\text{1st}} \equiv H^{\text{1st}}(P) - H^{\text{1st}}(0)$, where $H^{\text{1st}}(P)$ is the first principles tight-binding model for FeSe under P GPa in the tetragonal phase given by the WIEN2k software. The inter-layer hopping inte-

grals are dropped to obtain the two-dimensional model. Hereafter, we study the total Hamiltonian $H = H_0 + H^{\text{1st}}(P) + rH_U$. Here, we introduce H_0 by shifting the orbital level $\delta E_l(\Gamma), \delta E_l(X), \delta E_l(Y), \delta E_l(M)$ as $(-0.24, -0.38, 0.12, 0.5)$ for $l = 2$, $(-0.24, 0.12, -0.38, 0.5)$ for $l = 3$, and $(0.5, -0.24, -0.24, 0.2)$ for $l = 4$ in unit eV. Here, $M = (\pi, \pi)$. Figure S5 (a) shows the bandstructure for $P = 0, 2$, and 4 GPa given by the eigenvalues of $H_0 + H^{\text{1st}}(P)$. The FSs are sensitively modified by the following orbital levels given by $H^{\text{1st}}(P)$: $E_2(\Gamma) = E_3(\Gamma)$, $E_2(Y) = E_3(X)$, $E_4(X)$, and $E_4(M)$. These P -dependences are shown in Fig. S5 (b). Among them, $E_4(M)$ shows the most prominent P -dependence. The obtained FSs for $P = 0$ and 2 GPa are shown in Figs. S5 (c) and (d), respectively. Since the top of the xy -orbital hole-band at $P = 0$ is -40 meV in the present model, the hFS3 appears at $P = 2\text{ GPa}$.

Figure S6 (a) shows the Stoner factors $\alpha_{S,C}$ obtained by the SC-VC theory for $r = 0.263$ at $T = 20\text{meV}$. At ambient pressure, α_C is much larger than α_S . For $P \lesssim 2\text{ GPa}$, α_C decreases in proportion to P , reflecting the decrease of $X_{yz}^c(\mathbf{0}) \sim \chi_{yz}^s(\mathbf{Q})$. In this model, the minimum of α_C is 0.86 at $P = 2.5\text{ GPa}$, which becomes much smaller than that in Fig. 2 (e) in the main text ($\alpha_C = 0.925$ at $\Delta E_{xy} = 0.1\text{eV}$). For $P \gtrsim 2\text{ GPa}$, the hFS3 appears, and then α_S starts to increase due to the nesting between hFS3 and eFS1,2. In addition, α_C also starts to increase for $P > 2.5\text{ GPa}$ since $\chi_{xy}^s(\mathbf{q})$ also contribute to the ‘‘AL-term on yz -orbital due to $|\Lambda_{3,3;4,4;4,4}^0|^2 T \sum_{\mathbf{q}} \{\chi_{xy}^s(\mathbf{q})\}^2$ ’’. These results are essentially equivalent to Fig. 2 (f) in the main text.

Figure S6 (b) shows the eigenvalue of the gap equation obtained for V^{tot} (λ^{tot}) and that for V^Λ (λ^Λ). Both V^{tot} and V^Λ includes the beyond-Migdal-Eliashberg effects discussed in the main text. For comparison, we also show $\lambda(\text{Migdal})$. For $P = 4\text{ GPa}$, the s_\pm -wave state with sign reversal between electron- and hole-pockets is obtained for V^Λ as shown in Fig. S6 (c). In contrast, the ‘‘ s_{++} -wave state without sign reversal’’ is obtained for the total pairing interaction V^{tot} as shown in Fig. S6 (d), since V^{cross} gives large inter-pocket attractive interaction: These results are essentially equivalent to Figs. 3 (f) and (g) in the main text.

The low-energy bandstructure of H_0 introduced in this section is very similar to that in the main text near the Fermi level ($|\mu - \epsilon| < 0.5\text{ eV}$). (Note that the bandstructure away from the Fermi level is unknown because of the broadening of the ARPES spectra.) Even if H_0 in the main text are used, the obtained P -dependences of the Stoner factors in Fig. S6 (a) are qualitatively unchanged.

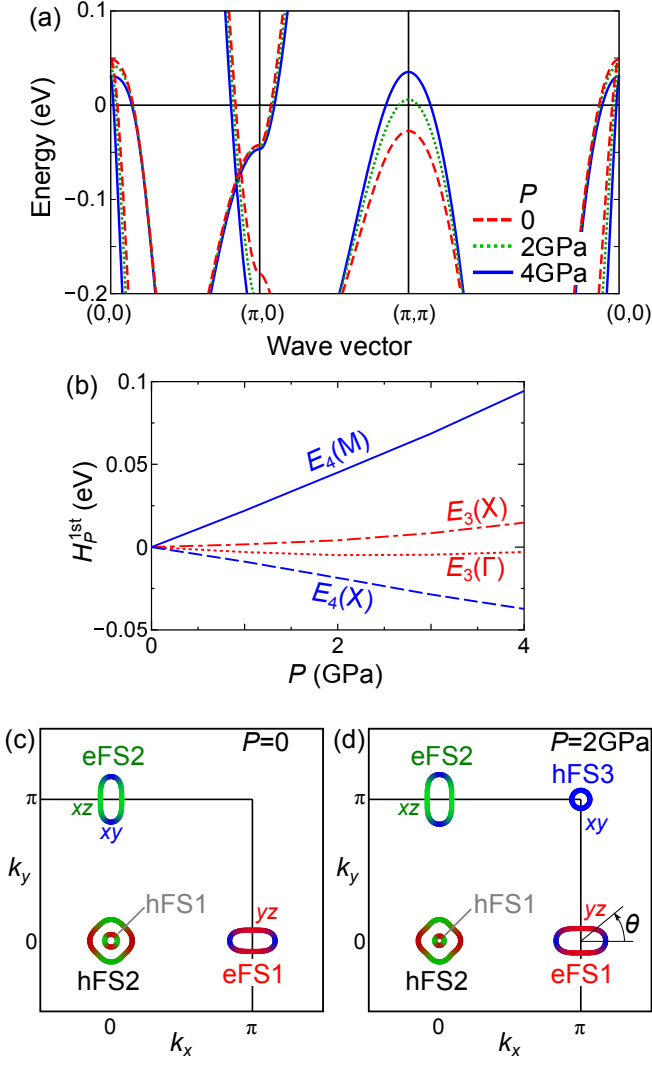


FIG. S5: (color online) (a) Band structure of the two-dimensional FeSe model $H_0 + H_P^{1st}$ at $P = 0, 2,$ and 4 GPa. (b) $E_3(\Gamma)$, $E_3(X)$, $E_4(X)$ and $E_4(M)$ given by $H_P^{1st}(P)$. (c) FSs at $P = 0$ GPa. (d) FSs at $P = 2$ GPa: The $hFS3$ is the xy -orbital hole-pocket.

E: Pairing interaction beyond the Migdal-Eliashberg theory

In conventional Migdal-Eliashberg (ME) gap equation, the pairing interaction is given by the single-fluctuation exchange process, and the VC for the coupling constant (U -VC) is dropped. In the main text, we studied the gap equation by including the pairing interaction beyond the ME formalism, such as the U -VC and the double-fluctuation exchange processes $V^{\text{cross}}(\mathbf{k}, \mathbf{p})$. Here, we explain the analytic expressions for these beyond ME processes [13].

The analytic expression of V^Λ in Fig. 3 (b) in the main

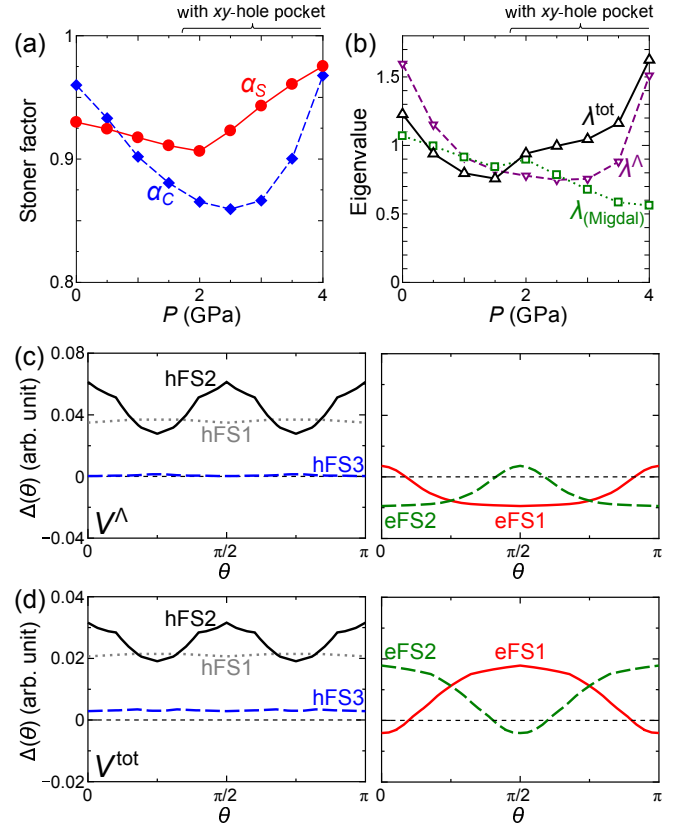


FIG. S6: (color online) (a) Stoner factors $\alpha_{S,C}$ for $P = 0 \sim 4$ GPa, at $T = 20\text{meV}$ and $r = 0.263$. (b) Eigenvalues λ^Λ and λ^{tot} as functions of P . For comparison, we also show $\lambda_{(\text{Migdal})}^\Lambda$. (c) s_{\pm} -wave gap given by V^Λ at $P = 4$ GPa. (d) s_{++} -wave gap given by V^{tot} at $P = 4$ GPa. Numerical study is performed in the nonmagnetic state.

text is

$$\hat{V}^\Lambda(k, p) = \frac{3}{2}\hat{I}^{\Lambda,s}(k, p) - \frac{1}{2}\hat{I}^{\Lambda,c}(k, p) - \hat{U}^{0s}, \quad (\text{S1})$$

where

$$\hat{I}^{\Lambda,x}(k, p) = \hat{\Lambda}^x(k, p)\hat{I}^x(k-p)\hat{\Lambda}^x(-k, -p). \quad (\text{S2})$$

Here, Λ^x ($x = s, c$) is the U -VC shown in Fig. 3 (d). From now on, we explain the analytic expressions for the U -VC due to the Maki-Thompson (MT) and Aslamazov-Larkin (AL) processes which were already given in Ref. [13]. First, we explain the charge- and spin-channel MT-terms:

$$\Lambda_{l,l';m,m'}^{\text{MT},c}(k, k') = \frac{T}{2} \sum_p \sum_{a,b} \{I_{b,l';a,l}^c(p) + 3I_{b,l';a,l}^s(p)\} \times G_{a,m}(k+p)G_{m',b}(k'+p), \quad (\text{S3})$$

$$\Lambda_{l,l';m,m'}^{\text{MT},s}(k, k') = \frac{T}{2} \sum_p \sum_{a,b} \{I_{b,l';a,l}^c(p) - I_{b,l';a,l}^s(p)\}$$

$$\times G_{a,m}(k+p)G_{m',b}(k'+p), \quad (\text{S4})$$

where $\hat{I}^x(q) = \hat{U}^{0x}\hat{\chi}^x(q)\hat{U}^{0x} + \hat{U}^{0x}$.

Next, we explain the charge- and spin-channel AL-terms:

$$\begin{aligned} \Lambda_{l,l';m,m'}^{\text{AL},c}(k,k') &= \frac{T}{2} \sum_p \sum_{a,b,c,d,e,f} G_{a,b}(k'-p) \Lambda_{m,m';c,d,e,f}^{0'}(k-k',p) \\ &\times \{ I_{l,a;c,d}^c(k-k'+p) I_{b,l';e,f}^c(-p) \\ &+ 3I_{l,a;c,d}^s(k-k'+p) I_{b,l';e,f}^s(-p) \}, \end{aligned} \quad (\text{S5})$$

$$\begin{aligned} \Lambda_{l,l';m,m'}^{\text{AL},s}(k,k') &= \frac{T}{2} \sum_p \sum_{a,b,c,d,e,f} G_{a,b}(k'-p) \Lambda_{m,m';c,d,e,f}^{0'}(k-k',p) \\ &\times \{ I_{l,a;c,d}^c(k-k'+p) I_{b,l';e,f}^s(-p) \\ &+ I_{l,a;c,d}^s(k-k'+p) I_{b,l';e,f}^c(-p) \} \\ &+ \delta \Lambda_{l,l';m,m'}^{\text{AL},s}(k,k'), \end{aligned} \quad (\text{S6})$$

where $\Lambda_{m,m';c,d;g,h}^{0'}(q,p) \equiv \Lambda_{c,h;m,g;d,m'}^0(q,p) + \Lambda_{g,d;m,c;h,m'}^0(q,-p-q)$. $\hat{\Lambda}^0$ is the three-point vertex in Fig. 2 (b) in the main text. The last term in Eq. (S6) is given as

$$\begin{aligned} \delta \Lambda_{l,l';m,m'}^{\text{AL},s}(k,k') &= T \sum_p \sum_{a,b,c,d,e,f} G_{a,b}(k'-p) \\ &\times I_{l,a;c,d}^s(k-k'+p) I_{b,l';e,f}^s(-p) \Lambda_{m,m';c,d,e,f}^{0''}(k-k',p), \end{aligned} \quad (\text{S7})$$

which is found to be very small [9]. Here, $\Lambda_{m,m';c,d;g,h}^{0''}(q,p) \equiv \Lambda_{c,h;m,g;d,m'}^0(q,p) - \Lambda_{g,d;m,c;h,m'}^0(q,-p-q)$.

The (U^0) -linear terms in Eqs. (S3) and (S4) should be dropped to avoid the double counting of the RPA-type diagrams. We also carefully drop the double counting $(U^0)^2$ -terms included in both MT and AL terms. We verified numerically that the large charge-channel U -VC ($|\Lambda^c|^2 \gg 1$) originates from the χ^s -square term in Eq. (S5). We also verified that the relation $|\Lambda^s|^2 \ll 1$ is realized mainly by the $(U^0)^2$ -term [13].

Next, we explain the double-fluctuation exchange process $V^{\text{cross}}(k,p)$, which gives sizable pairing interaction in Fe-based superconductors [13]. It is schematically expressed as Fig. 3 (c) in the main text. Physically,

$V^{\text{cross}}(k,p)$ represents the pairing interaction due to the ‘‘multi-fluctuation exchange processes’’. This term is expressed as [13]

$$\begin{aligned} V_{l,l';m,m'}^{\text{cross}}(k,p) &= \frac{T}{4} \sum_q \sum_{a,b,c,d} G_{a,b}(p-q) G_{c,d}(-k-q) \\ &\times \{ 3I_{l,a;m,d}^{s'}(k-p+q) I_{b,l';c,m'}^{s'}(-q) \\ &+ 3I_{l,a;m,d}^{s'}(k-p+q) I_{b,l';c,m'}^{c'}(-q) \\ &+ 3I_{l,a;m,d}^{c'}(k-p+q) I_{b,l';c,m'}^{s'}(-q) \\ &- I_{l,a;m,d}^{c'}(k-p+q) I_{b,l';c,m'}^{c'}(-q) \}, \end{aligned} \quad (\text{S8})$$

where we put $\hat{I}^x = \hat{I}^x - \hat{U}^{0x}$ to avoid the double counting of diagrams included in other terms. According to Eq. (S8), $V_{m,m;m,m}^{\text{cross}}$ can take large negative value when the spin fluctuations develop on the m -orbital [13].

-
- [1] J. N. Millican, D. Phelan, E. L. Thomas, J. B. Leão, and E. Carpenter, *Solid State Commun.* **149**, 707 (2009).
 - [2] A. E. Böhrer, F. Hardy, F. Eilers, D. Ernst, P. Adelman, P. Schweiss, T. Wolf, and C. Meingast, *Phys. Rev. B* **87**, 180505(R) (2013).
 - [3] K. Kuroki, H. Usui, S. Onari, R. Arita, and H. Aoki, *Phys. Rev. B* **79**, 224511 (2009).
 - [4] Y. Mizukami and T. Shibauchi, private communication.
 - [5] Y. Suzuki, T. Shimojima, T. Sonobe, A. Nakamura, M. Sakano, H. Tsuji, J. Omachi, K. Yoshioka, M. Kuwata-Gonokami, T. Watashige, R. Kobayashi, S. Kasahara, T. Shibauchi, Y. Matsuda, Y. Yamakawa, H. Kontani, and K. Ishizaka, *Phys. Rev. B* **92**, 205117 (2015).
 - [6] Y. Yamakawa, S. Onari, and H. Kontani, *Phys. Rev. X* **6**, 021032 (2016).
 - [7] T. Miyake, K. Nakamura, R. Arita, and M. Imada, *J. Phys. Soc. Jpn.* **79**, 044705 (2010).
 - [8] S. Onari, Y. Yamakawa, and H. Kontani, *Phys. Rev. Lett.* **116**, 227001 (2016).
 - [9] S. Onari and H. Kontani, *Phys. Rev. Lett.* **109**, 137001 (2012).
 - [10] Z. P. Yin, K. Haule, and G. Kotliar, *Nat. Mater.* **10**, 932 (2011).
 - [11] H. C. Xu, X. H. Niu, D. F. Xu, J. Jiang, Q. Yao, M. Abdel-Hafiez, D. A. Chareev, A. N. Vasiliev, R. Peng, and D. L. Feng, *Phys. Rev. Lett.* **117**, 157003 (2016).
 - [12] S. Kasahara, T. Yamashita, A. Shi, R. Kobayashi, Y. Shimoyama, T. Watashige, K. Ishida, T. Terashima, T. Wolf, F. Hardy, C. Meingast, H. v Löhneysen, A. Levchenko, T. Shibauchi, and Y. Matsuda, arXiv:1608.01829.
 - [13] Y. Yamakawa, and H. Kontani, arXiv:1611.05375.